INTERNATIONAL JOURNAL FOR NUMERICAL METHODS IN ENGINEERING
Int. J. Numer. Meth. Engng 2005; **64**:1575–1593
Published online 29 July 2005 in Wiley InterScience (www.interscience.wiley.com). DOI: 10.1002/nme.1409

A unified formulation for continuum mechanics applied to fluid–structure interaction in flexible tubes

C. J. Greenshields[1,*,†] and H. G. Weller[2]

[1]*Mechanical Engineering, University of Strathclyde, Glasgow G1 1XJ, U.K.*
[2]*OpenCFD Limited, The Mews Picketts Lodge, Picketts Lane, Salfords, Surrey RH1 5RG, U.K.*

SUMMARY

This paper outlines the development of a new procedure for analysing continuum mechanics problems with a particular focus on fluid–structure interaction in flexible tubes. A review of current methods of fluid–structure coupling highlights common limitations of high computational cost and solution instability. It is proposed that these limitations can be overcome by an alternative approach in which both fluid and solid components are solved within a single discretized continuum domain. A single system of momentum and continuity equations is therefore derived that governs both fluids and solids and which are solved with a single mesh using finite volume discretization schemes. The method is validated first by simulating dynamic oscillation of a clamped elastic beam. It is then applied to study the case of interest—wave propagation in highly flexible tubes—in which a predicted wave speed of 8.58 m/s falls within 2% of an approximate analytical solution. The method shows further good agreement with analytical solutions for tubes of increasing rigidity, covering a range of wave speeds from those found in arteries to that in the undisturbed fluid. Copyright © 2005 John Wiley & Sons, Ltd.

KEY WORDS: fluid–structure interaction; finite volume; continuum; transients; hemodynamics

1. INTRODUCTION

Fluid–structure interaction (FSI) is a term generally used to describe a dynamic system whose behaviour is influenced by the interaction of a moving fluid and a deforming solid structure. FSI is an important consideration in many engineering fields, for example, flow-induced vibration, noise, hydrodynamics and processing. This paper addresses the problem of fluid transients in flexible cylindrical tubes which is directly relevant to practical problems such as: hemodynamics; pressure surge in pipelines; impact of fluid-filled containers. The subject deals specifically with wave propagation due to disturbances in fluid flow and pressure. In a straight unconstrained

*Correspondence to: C. J. Greenshields, Mechanical Engineering, University of Strathclyde, Glasgow G1 1XJ, U.K.
†E-mail: chris.greenshields@strath.ac.uk

Received 17 March 2004
Revised 4 March 2005
Accepted 21 March 2005

section of tube the wave speed c can be approximated by the Korteweg equation [1]

$$c = \sqrt{\frac{K_\mathrm{f}}{\rho_\mathrm{f}} \left(1 + \frac{D}{t}\frac{K_\mathrm{f}}{E}\right)^{-1}} \tag{1}$$

where K_f and ρ_f are the bulk modulus and density of the fluid, respectively, D and t are the internal diameter and thickness of the tube, respectively, and E is the modulus of elasticity of the tube material. Equation (1) reflects the fact that FSI can be ignored in the analysis of perfectly rigid tubes, since as $E \to \infty$, c tends to the sound velocity for an unconfined fluid

$$c_0 = \sqrt{\frac{K_\mathrm{f}}{\rho_\mathrm{f}}} \tag{2}$$

For water at 20°C and atmospheric pressure, $K_\mathrm{f} = 2.2\,\mathrm{GPa}$ and $\rho_\mathrm{f} = 998\,\mathrm{kg/m^3}$ [2], and $c_0 = 1483\,\mathrm{m/s}$. Equation (1) provides reasonable predictions of wave speed in real, deformable structures, such as polymer pipes for water distribution in which, typically, $c \approx 500\,\mathrm{m/s}$. For extremely flexible tubes, such as rubber hoses and blood vessels, $E \ll K_\mathrm{f}$ and Equation (1) further approximates to

$$c_1 \approx \sqrt{\frac{E}{\rho_\mathrm{f}}\frac{t}{D}} \tag{3}$$

which is often referred to as the 'Moens–Korteweg' equation although it can be attributed to Young [3]. Wave speeds as low as 5 m/s are observed in human arteries, almost 300× lower than c_0 of blood.

The associated particle flow speed U_x along the tube axis x is given by Joukowsky's equation [4]

$$U_x = \frac{p}{\rho_\mathrm{f} c} \tag{4}$$

where p is the pressure difference across the wave front. A wave speed of 5 m/s can generate a flow speed of 1 m/s with only a modest pressure excursion of 5 kPa produced within the human cardiovascular system.

Equations (3) and (4) provide good approximation of wave and flow speeds in flexible tubes but only more involved solution methods, especially computational tools, can reveal the details of the flow and tube wall deformation. Currently, most attempts to produce the detailed solutions use simplifying assumptions that arguably do not reflect the physical behaviour of the problem. The aim of the work presented here is to develop and implement a numerical procedure for detailed analysis of fluid transients in flexible tubes which produces a representative solution, i.e. primarily one which is wave like. The requirements for the model are:

- the analysis is fully transient;
- both fluid and solid are treated as weakly compressible;
- no approximations, e.g. thin-wall assumptions, are made to the momentum or continuity equations for fluid and structure;
- 'full' coupling between fluid and structure as defined in the next section.

2. FLUID–STRUCTURE COUPLING

A major aspect of FSI analysis is the coupling of the fluid and structure components. The coupling involves an exchange of information, such as stresses, velocities and/or displacements, across the interface. The manner and timing of the information transfer dictates the level of coupling, often described as either 'weak' or 'strong'. In this paper the term 'full' is preferred to describe a level of coupling where, at any time, the solutions for both the fluid and solid domains have converged to a tight tolerance and are mutually consistent, for example, where the solution for fluid pressure at all points on the interface is identical to the normal traction on the solid boundary. Figure 1 splits different coupling schemes into three categories distinguished by: separate analysis methods for fluid and structure; a single analysis method; a single solution domain.

2.1. Separate analysis methods

The most common coupling schemes solve the individual fluid and structural problems using separate methods which are linked by a program that transfers information across the interface. Data transfer is not trivial, since the data structures contained within the two solution methods are likely to be different and an interpolation scheme is required when computational nodes of the fluid and solid meshes are not collocated along the interface. A fully transient solution with full coupling can only then be achieved by iterating to convergence between fluid and structure within each time step, requiring numerous stops and restarts of the solution methods. This approach is therefore extremely demanding on computational resources and involves the

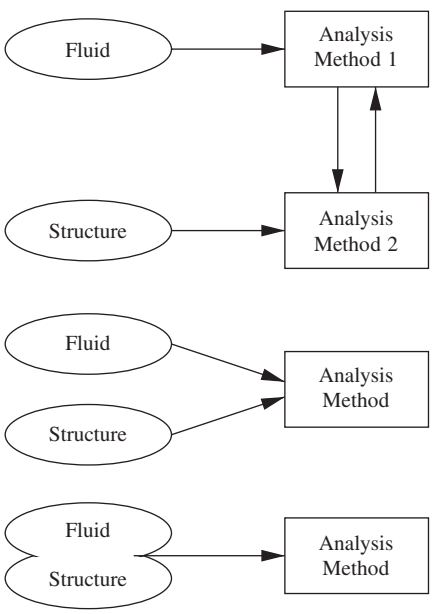

Figure 1. Fluid–structure coupling schemes: (from top) separate analysis methods; single analysis methods; a single solution domain.

use, maintenance and/or development of essentially three computational tools, i.e. for fluid, solid and interface. Consequently, when applying separate analysis methods to analyse blood flow, approximations are invariably introduced to simplify the analysis but at a cost to the detail and accuracy of the solution [5–11]. Apart from simply reducing the problem to one- or two dimensions, it is common to find: analytical wave propagation models; simplified wall motion models; thin-wall assumptions; incompressible flow; steady flow; and solutions with little or no coupling.

2.2. Single analysis method

An alternative approach is to treat the fluid and structure domains separately but solve them using a single method [12, 13]. The use of a single numerical tool enables an internal transfer of information at the fluid–structure interface through a single, common data structure and, therefore, without the additional burden of running and maintaining an interface program. It is thus significantly less costly than before to achieve full coupling with a converged solution over the complete fluid/structure system within each time step.

This approach has been shown to predict surge wave propagation in plastic pipes accurately and efficiently [13]. However, the convergence and stability of the procedure was found to be critically dependent on the choice of and manner in which variables are passed across the interface. The intuitive choice—passing pressure from the fluid to solid and wall velocity from solid to fluid—is particularly unstable in cases where the structure has a low modulus of elasticity in relation to the compressibility of the fluid or, in our case of interest, where the approximation $3E < K_f$ holds. Instability can be overcome by underrelaxation of the interface coupling but this is fairly impractical for geometries which are even moderately complex. Moreover, the instability is inherent when using any iterative procedure that solves separate fluid and structural components with data transfer across the interface, casting doubt over the efficacy of separate analysis methods to produce a fully coupled, transient solution for such cases.

2.3. Single fluid–structure domain

The third type of coupling treats the whole fluid–structure domain as a single entity and describes its behaviour by a single set of equations which are solved using a single numerical method. In computational terms, this means that instead of solving different systems of equations for two separate meshes for the fluid and structure, the complete fluid/structure system is described by a single mesh and solved using one set of equations. The interface is then contained within the solution domain itself and the coupling is inherently full. This is the basis of the FSI method presented here, which begins with a derivation of a single set of equations to describe both fluid and solid in the next section. The subsequent section outlines the finite volume (FV) method using a segregated, iterative solution procedure which makes it ideal for non-linear, transient problems. It is primarily this feature that has made FV the preferred method for commercial computational fluid dynamics; its use in structural applications is less common [14–16], but of interest especially for non-linear problems particularly those involving complex physics including, notably, FSI [17–19].

3. MATHEMATICAL FORMULATION

The work is concerned with a unified mathematical description for fluid and solid in which thermal contributions are ignored. The behaviour of a continuum in an Eulerian frame of reference is governed by the following equations [20]:

- mass balance, or continuity equation

$$\frac{\partial \rho}{\partial t} + \nabla \cdot (\rho \mathbf{U}) = 0 \tag{5}$$

- momentum balance (neglecting body forces)

$$\frac{\partial \rho \mathbf{U}}{\partial t} + \nabla \cdot (\rho \mathbf{U}\mathbf{U}) = \nabla \cdot \boldsymbol{\sigma} \tag{6}$$

where ρ is the density, $\mathbf{U}$ is the velocity and $\boldsymbol{\sigma}$ is the stress tensor. Up to this point, both fluid and solid obey the same principles of continuum mechanics; it is in their constitutive models that they differ. In this work we assume that the solid is linear elastic, or Hookean, and undergoes only small strain deformation and that the fluid is linear viscous, or Newtonian.

3.1. Constitutive models for fluid and solid

The constitutive model for a Newtonian fluid is

$$\boldsymbol{\sigma} = 2\eta \operatorname{dev}(\mathbf{D}) - p\mathbf{I} \tag{7}$$

where η is the dynamic viscosity, the deformation rate tensor $\mathbf{D}$ is the symmetric part of the velocity gradient, $\mathbf{D} \equiv \operatorname{symm}(\nabla \mathbf{U}) \equiv \frac{1}{2}[\nabla \mathbf{U} + (\nabla \mathbf{U})^{\mathrm{T}}]$, with the deviatoric component of $\mathbf{D}$, $\operatorname{dev}(\mathbf{D}) \equiv \mathbf{D} - \frac{1}{3}\operatorname{tr}(\mathbf{D})\mathbf{I}$; and, pressure p is the hydrostatic component of the stress tensor defined as positive in compression, such that the stress tensor can be decomposed into its deviatoric and hydrostatic components by

$$\boldsymbol{\sigma} = \operatorname{dev}(\boldsymbol{\sigma}) + \tfrac{1}{3}\operatorname{tr}(\boldsymbol{\sigma})\mathbf{I} = \operatorname{dev}(\boldsymbol{\sigma}) - p\mathbf{I} \tag{8}$$

Equations (6) and (7) combine to produce the following momentum equation with p and $\mathbf{U}$ becoming the primary solution variables:

$$\frac{\partial \rho \mathbf{U}}{\partial t} + \nabla \cdot (\rho \mathbf{U}\mathbf{U}) = \nabla \cdot [2\eta \operatorname{dev}(\operatorname{symm}(\nabla \mathbf{U}))] - \nabla p \tag{9}$$

By contrast, the constitutive model for a Hookean solid relates $\boldsymbol{\sigma}$ to strain $\mathbf{E}$ according to [20]

$$\operatorname{dev} \boldsymbol{\sigma} = 2\mu \operatorname{dev}(\mathbf{E}) \tag{10}$$

where the shear modulus $\mu = E/[2(1 + \nu)]$ and ν is Poisson's ratio. It is usual to solve for displacement in solid dynamics since $\mathbf{E}$ is a function of displacement gradient.

Our intended unified description requires that we solve for the same primitive variables in both fluids and solids. The most feasible choice is to solve for $\mathbf{U}$ since $\mathbf{U}$ is inherent to fluid flow: it would be highly impractical, for example, to rewrite the convective derivative $\nabla \cdot (\rho \mathbf{U}\mathbf{U})$

in Equation (9) in terms of displacements. We therefore preserve the system of fluid equations and modify the structure equations to a form containing p and $\mathbf{U}$.

3.2. A unified momentum equation for fluid and solid

The main challenge is to produce a momentum equation for a Hookean solid in a form similar to Equation (9). The first step is to decompose $\mathrm{dev}(\boldsymbol{\sigma})$ of Equation (10) into the sum of a reference, or initial, deviatoric stress $\mathrm{dev}(\boldsymbol{\sigma}_0)$ at time $t = \tau_0$ and an accumulated deviatoric stress between $t = \tau_0$ and the current time τ_n, such that

$$\mathrm{dev}(\boldsymbol{\sigma}) = \int_{\tau_0}^{\tau_n} \mathrm{dev}(\dot{\boldsymbol{\sigma}})\,\mathrm{d}t + \mathrm{dev}(\boldsymbol{\sigma}_0) \tag{11}$$

In order to derive a momentum equation in the form of Equation (9), we express the integral in Equation (11) by a quadrature formula using appropriate weighting functions w_i at discrete sampling points $i = 0, 1, \ldots, n$ corresponding to times $\tau_0, \tau_1, \ldots, \tau_n$ as follows:

$$\int_{\tau_0}^{\tau_n} \mathrm{dev}(\dot{\boldsymbol{\sigma}})\,\mathrm{d}t = w_n\,\mathrm{dev}(\dot{\boldsymbol{\sigma}})_n + \sum_{i=0}^{n-1} w_i\,\mathrm{dev}(\dot{\boldsymbol{\sigma}})_i \tag{12}$$

This time integration of deviatoric stress is illustrated in Figure 2 and, in the context of a transient numerical solution scheme, consists of a term $w\,\mathrm{dev}(\dot{\boldsymbol{\sigma}}) \equiv w_n\,\mathrm{dev}(\dot{\boldsymbol{\sigma}})_n$ at the current, unsolved time and a summation ($i = 0, 1, \ldots, n-1$) representing an accumulation of stress at previous, solved times. The latter can be combined with $\mathrm{dev}(\boldsymbol{\sigma}_0)$ to produce a deviatoric stress $\boldsymbol{\Sigma}$ accumulated up to the current time

$$\boldsymbol{\Sigma} = \sum_{i=0}^{n-1} w_i\,\mathrm{dev}(\dot{\boldsymbol{\sigma}})_i + \mathrm{dev}(\boldsymbol{\sigma}_0) \tag{13}$$

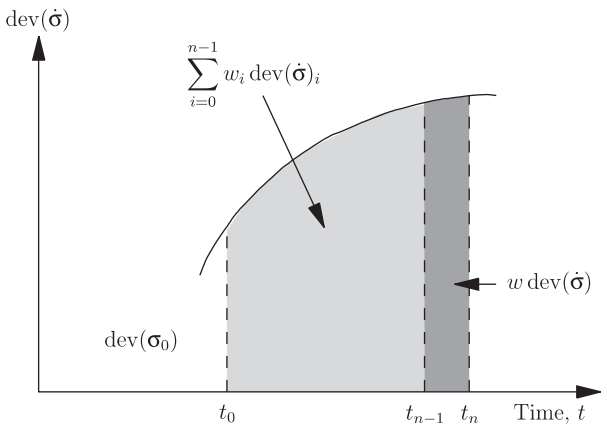

Figure 2. Integration of the rate of deviatoric stress.

so that Equation (11) becomes

$$\mathrm{dev}(\boldsymbol{\sigma}) = w\,\mathrm{dev}(\dot{\boldsymbol{\sigma}}) + \boldsymbol{\Sigma} \tag{14}$$

An expression for $\mathrm{dev}(\dot{\boldsymbol{\sigma}})$ can be derived from the time derivative of Equation (10), noting that, for small strain deformation, $\mathbf{D} = \dot{\mathbf{E}}$:

$$\mathrm{dev}(\dot{\boldsymbol{\sigma}}) = 2\mu\,\mathrm{dev}(\mathbf{D}) \tag{15}$$

An alternative form of the constitutive law for a Hookean solid can thus be derived by combining Equations (8), (14), (15) and the definition of $\mathbf{D}$:

$$\boldsymbol{\sigma} = 2\mu w\,\mathrm{dev}(\mathrm{symm}(\nabla\mathbf{U})) + \boldsymbol{\Sigma} - p\mathbf{I} \tag{16}$$

This expression for stress can be substituted into Equation (6) to produce a momentum equation for a Hookean solid in terms of velocity and pressure:

$$\frac{\partial \rho\mathbf{U}}{\partial t} + \nabla\cdot(\rho\mathbf{U}\mathbf{U}) = \nabla\cdot[2\mu w\,\mathrm{dev}(\mathrm{symm}(\nabla\mathbf{U}))] - \nabla p + \nabla\cdot\boldsymbol{\Sigma} \tag{17}$$

Equation (17) has the same form as the Equation (9) for a Newtonian fluid, but with an additional term $\nabla\cdot\boldsymbol{\Sigma}$ representing the accumulation (history) of the deviatoric component of stress in the solid over time and with the μw coefficient replacing η. Let us define a continuum viscosity field

$$\mu_c = (1-\alpha)\eta + \alpha\mu w \tag{18}$$

where the phase fraction:

$$\alpha = \begin{cases} 0 & \text{for a fluid} \\ 1 & \text{for a solid} \end{cases} \tag{19}$$

We can then write a momentum equation for generic fluid/solid system as

$$\frac{\partial \rho\mathbf{U}}{\partial t} + \nabla\cdot(\rho\mathbf{U}\mathbf{U}) = \nabla\cdot[\mu_c\,\mathrm{dev}(\mathrm{symm}(\nabla\mathbf{U}))] - \nabla p + \nabla\cdot\boldsymbol{\Sigma} \tag{20}$$

where $\boldsymbol{\Sigma}$ can be calculated by premultiplying Equation (13) by α, i.e. $\boldsymbol{\Sigma} = \mathbf{0}$ for a fluid and is non-zero for a solid. Equation (20) can thus describe both fluid and solid within a single domain, or mesh, according to Section 2.3, where α indicates the fluid and solid regions within the domain.

3.3. Closing the system of equations for fluid and solid

A generic continuity equation for a weakly compressible continuum is formulated in terms of p using Equation (5) and the barotropic relationship between p and ρ

$$\frac{\partial \rho}{\partial p} = \frac{\rho}{K} \tag{21}$$

which can be linearized to

$$\rho \approx \rho_0[1 + (p - p_0)/K] \tag{22}$$

for small variations in pressure about a reference pressure p_0. Here, K denotes the bulk modulus field that can be evaluated by

$$K = (1 - \alpha)K_f + \alpha K_s \tag{23}$$

where K_s is the solid bulk modulus, often derived from E and v by $K_s = E/[3(1 - 2v)]$.

This relationship linking ρ and p closes the system of equations and the description of a problem is completed with: the definition of a solution domain; the specification of values of all dependent variables throughout the solution domain at the initial instant of time; specification of boundary conditions at all times either by the value of the dependent variable or the gradient of the dependent variable normal to the boundary.

4. COMPUTATIONAL METHOD

This work uses the FV method of discretization that will be described briefly here. Firstly, the time domain is discretized into a set of time steps and the spatial domain is divided into a number of contiguous control volumes, or cells, with 'f' faces as shown in Figure 3. All dependent variables and material properties are stored at each cell centroid 'P'.

Each term in the system of differential equations is first expressed within an integral over a cell volume V, with divergence and gradient terms then being converted to integrals over the cell surface S using the generalized form of Gauss's theorem. The combined set of volume and surface integrals is then linearized using the schemes briefly described below:

- The time discretization scheme is implicit using a derivative evaluated over two time levels [21].

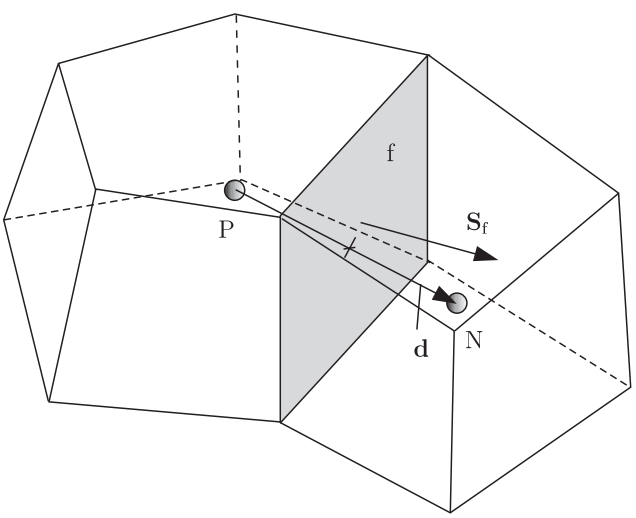

Figure 3. Finite volume discretization.

- The face velocity $\mathbf{U}_\mathrm{f}$ in the convection term is calculated using the Gamma differencing scheme [22] which locally blends second order accurate central differencing with unconditionally bounded upwind differencing to ensure boundedness.
- Values of dependent variables other than $\mathbf{U}$ are interpolated linearly from cell centres to cell faces.
- The face gradient discretization is implicit for orthogonal meshes

$$\mathbf{S}_\mathrm{f} \bullet (\nabla \mathbf{U})_\mathrm{f} = |\mathbf{S}_\mathrm{f}| \frac{\mathbf{U}_\mathrm{N} - \mathbf{U}_\mathrm{P}}{|\mathbf{d}|}$$

  where $\mathbf{S}_\mathrm{f}$ is the face area vector pointing out of the cell of interest, and $\mathbf{d}$ is the vector between the centre of that cell P and the centre of a neighbouring cell N.

4.1. Solution procedure

An algorithm similar to PISO [23] is adopted to ensure that the velocity field satisfies the continuity equation and proceeds as follows. The momentum equation (20) is first solved in which the non-linear convection term is linearized by substituting the existing flux field $F = \mathbf{S}_\mathrm{f} \bullet (\rho \mathbf{U})_\mathrm{f}$ calculated from the previous time step (Equation (26)), with the other $\mathbf{U}$ treated implicitly. The additional term $\nabla \bullet \boldsymbol{\Sigma}$ is present in the cells belonging to the solid region. In this work, a fixed time step Δt was used and $\boldsymbol{\Sigma}$ is calculated using the trapezoid rule, hence, $w(0) = w(t) = \Delta t/2$ and $w(\Delta t), w(2\Delta t), \ldots, w(t - \Delta t) = \Delta t$. The implementation is second order accurate in time and inherently simple since, at the beginning of a new time step, $\boldsymbol{\Sigma}$ is updated by the addition of a contribution from the previous time step only.

The momentum equation can be expressed in the form

$$a_\mathrm{P} \mathbf{U}_\mathrm{P} = \mathbf{H}(\mathbf{U}) - \nabla p \tag{24}$$

where a_P represents the coefficient for each individual component of the velocity vector and the $\mathbf{H}(\mathbf{U})$ operator contains all the matrix coefficients of cell neighbours multiplied by their corresponding velocities, and source terms other than those from the pressure gradient. The solution now enters a loop where the $\mathbf{H}(\mathbf{U})$ operator is formulated from the newly calculated velocity field and used to solve an equation for pressure derived from mass conservation (5), the barotropic relationship (22) and the momentum equation (24). Assuming K, ρ_0 and p_0 are constant in time and space, this gives

$$\underbrace{\frac{\partial(\psi p)}{\partial t} + \nabla \bullet \psi \frac{\mathbf{H}(\mathbf{U})}{a_\mathrm{P}} p - \nabla \bullet \frac{\rho}{a_\mathrm{P}} \nabla p}_{\text{implicit}} + \underbrace{\nabla \bullet (\rho_0 - \psi p_0) \frac{\mathbf{H}(\mathbf{U})}{a_\mathrm{P}} \psi}_{\text{explicit}} = 0 \tag{25}$$

where $\psi = \rho_0 / K$. The $\nabla \bullet (\nabla p)$ term is discretized using the procedure described by Rhie and Chow [24]. Explicit terms in Equation (25) are then updated to make them consistent with the new pressure field as follows:

- The velocity field is corrected using Equation (24) where $\mathbf{H}(\mathbf{U})$ is treated explicitly;
- The density field is updated using Equation (22).

We then return to the beginning of the loop and solve the pressure equation in which the $\mathbf{H}(\mathbf{U})$ operator has been recalculated with the new velocity field. We iterate around the loop

until a predetermined tolerance is reached; at the end of the loop, a conservative flux field is calculated by

$$F = \mathbf{S}_\mathrm{f} \bullet (\rho \mathbf{U})_\mathrm{f} = \mathbf{S}_\mathrm{f} \bullet \rho_\mathrm{f} \left[\left(\frac{\mathbf{H}(\mathbf{U})}{a_\mathrm{P}} \right)_\mathrm{f} - \left(\frac{1}{a_\mathrm{P}} \right)_\mathrm{f} (\nabla p)_\mathrm{f} \right] \tag{26}$$

for use in the momentum equation at the beginning of the next time step. The discretization procedure reduces our integral equations to a set of linear vector equations which are solved in a segregated manner, where each component of the dependent variable is solved separately, treating inter-component coupling terms explicitly, i.e. to solve U_x (in a Cartesian system) we assign the values of U_y and U_z from the previous iteration. The equations are solved using the Biconjugate Gradient method [25].

4.2. Boundary conditions and computer implementation

The test cases use boundary condition types commonly implemented in the FV method, such as the specification of a fixed value or gradient on the boundary [16]. However, the implementation of a specified traction boundary condition for the solid requires some care in the velocity/pressure formulation. The applied traction is directly added to the force balance for a CV with a face belonging to the traction boundary. The condition is effectively a specification of a Neumann condition on velocity on the boundary, i.e. specifying the normal gradient which can be evaluated from the balance between the applied and internal stresses. The velocity gradient is evaluated and used to calculate the boundary pressure through the continuity equation providing a Dirichlet boundary condition to solve the pressure equation.

The formulation was implemented into the Open Source Field Operation and Manipulation (OpenFOAM) C++ library [26]. OpenFOAM is an object-oriented programming environment for generating continuum mechanics applications using arbitrary unstructured 3D meshes defined in a rectangular Cartesian co-ordinate system.

5. MODEL VALIDATION

The numerical technique presented, which includes an algorithm similar to PISO, is widely adopted in fluid dynamics and therefore requires no validation with respect to fluid problems. However, the technique has never been used for structural or FSI applications and is therefore first validated on a purely structural problem before moving onto our FSI problem of interest.

5.1. Undamped vibration of a short beam in bending

The model was validated on a transient problem of bending of a short, 2-dimensional beam presented in Figure 4. The beam dimensions were length $l = 20\,\mathrm{m}$ and height $h = 5\,\mathrm{m}$. The mechanical properties were $E = 4.00\,\mathrm{GPa}$, Poisson's ratio $\nu = 0.32$, so that $K_\mathrm{s} = 3.70\,\mathrm{GPa}$ and $\mu = 1.51\,\mathrm{GPa}$. The density was $\rho_\mathrm{s} = 1450\,\mathrm{kg/m^3}$. The initial conditions throughout the domain and across all boundaries were $p = 0\,\mathrm{Pa}$, $\mathbf{U} = \mathbf{0}\,\mathrm{m/s}$ and $\boldsymbol{\Sigma} = \mathbf{0}\,\mathrm{Pa}$. The beam was fully constrained at one end and subjected to a suddenly applied shear stress $\tau = 1\,\mathrm{MPa}$ across the other end boundary face, with the upper and lower faces being traction free. The solver was executed in two dimensions only so that with no deformation in the third, out-of-plane, dimension, the problem was effectively treated as plane strain.

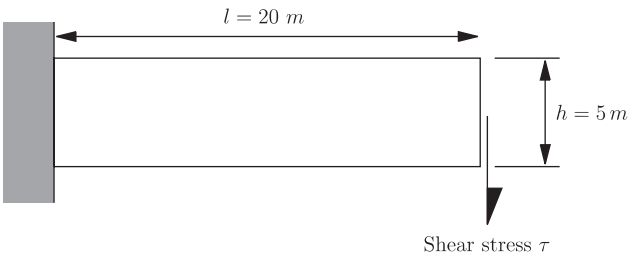

Figure 4. Beam bending case used for model validation.

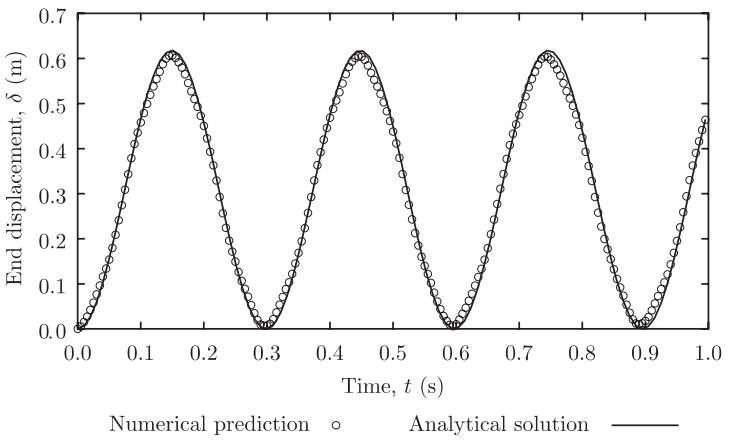

Figure 5. Vibration of a simple beam.

The test case used a mesh of 320 × 80 cells and a time step of $\Delta t = 20\,\mu s$, corresponding to a maximum wave speed Courant number Co of 0.5, where $Co = c_s(\Delta t/\Delta s)$, Δs is the minimum cell dimension, and the unconfined solid wave speed $c_s = \sqrt{E/\rho_s}$. Figure 5 compares the predicted displacement of the mid-point of the applied shear face, sampled every 250 time steps, with an analytical solution for the dynamics of an undamped clamped-free beam using the well-known assumptions of 1D beam theory with a correction for longitudinal shear deformation. The solution gives sinusoidal oscillation of the beam about a mean, or equilibrium, end displacement given by [27]

$$\bar{\delta} = \frac{4\tau}{E}\frac{l^3}{h^2}(1-\nu^2)\left[1+\frac{3}{4}(1+\nu)\left(\frac{h}{l}\right)^2\right] \tag{27}$$

at frequency of

$$\omega_n = \mu_n^2\sqrt{\frac{E}{12\rho_s}}\frac{h}{l^2} \tag{28}$$

where μ_n is the eigenvalue for mode n. In the test case, $\bar{\delta} = 0.309\,\text{m}$ and, for mode 1 ($n = 1$), $\mu = 1.875$ [28] and the frequency $f = \omega_1/2\pi = 3.35\,\text{Hz}$.

The predicted frequency was 3.37 Hz, within 0.5% of the analytical solution and the predicted mean displacement was 0.303 m, within 2.0% of the analytical solution. The numerical dissipation is small with the amplitude of oscillation dropping by only 0.5% per cycle.

5.2. FSI in a straight flexible tube

A test case of wave propagation in a straight flexible tube was chosen that causes problems of numeric instability with conventional coupling schemes using separate meshes for fluid and solid, as described previously [13]. The properties and basic geometry were also selected to be representative of blood flow in a large artery [29]: $D = 20\,\text{mm}$; $t = 2\,\text{mm}$; length $l = 100\,\text{mm}$; $E = 1.00\,\text{MPa}$ and $v = 0.3$, so that the wall bulk modulus $K_\text{s} = 833\,\text{kPa}$ and $\mu = 385\,\text{kPa}$; $\rho_\text{s} = 1000\,\text{kg/m}^3$; fluid viscosity $\eta = 0.004\,\text{Ns/m}^2$, density $\rho_\text{f} = 1000\,\text{kg/m}^3$ and bulk modulus $K_\text{f} = 2.2\,\text{GPa}$.

The test case is axisymmetric and therefore only requires a solution in 2D. The mesh is shown in Figure 6 with n_t cells along the tube length, n_f cells across the fluid cross-section and n_s cells across the solid domain. Five meshes were used in the study with different refinements; expressed as '$n_\text{t} - n_\text{f} - n_\text{s}$', the mesh sizes were 20-10-2, 30-20-3, 50-30-5, 70-40-7 and 90-50-9. The initial conditions throughout the domain and across all boundaries were $p = 0$ Pa, $\mathbf{U} = \mathbf{0}\,\text{m/s}$ and $\boldsymbol{\Sigma} = \mathbf{0}\,\text{Pa}$. Wave propagation was initiated at the left end of the tube by application of a fixed step change in pressure to $p = 5\,\text{kPa}$. Each analysis was run using a time step to ensure $Co < 1$, namely: 0.2 μs for the 20-10-2 and 30-20-3 meshes; 0.1 μs for the 50-30-5 mesh; 0.05 μs for the 70-40-7 and 90-50-9 meshes. The left and right tube wall boundaries were planes of symmetry and the outer wall was zero traction. The fluid boundaries were both fixed pressure and zero velocity gradient.

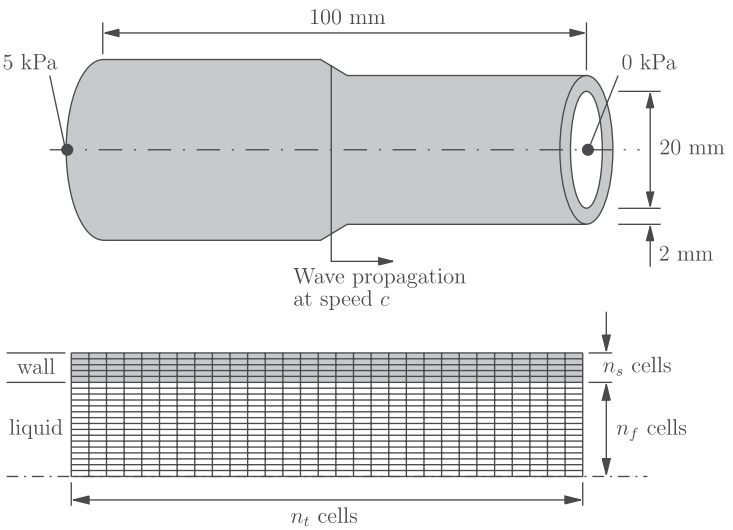

Figure 6. Schematic of tube geometry.

The simulation predicts wave propagation along the flexible tube which is presented in Figures 7–10 for the 70-40-7 case. The principal feature of wave propagation is radial wall motion which is shown in Figure 7. The wave propagates along the tube as a front behind which there is some overshoot and oscillation in the wall deflection which damps quite rapidly to a constant steady state $\approx D^2 p/4Et = 0.25$ mm over a few cycles. The simulated frequency is estimated at 318 Hz from the length of the first oscillation behind the wave front ≈ 27 mm, and the wave speed ≈ 8.58 m/s (evaluated later). An analytical solution for frequency, derived from the circumferential stiffness of the tube, its mass and an 'equivalent'

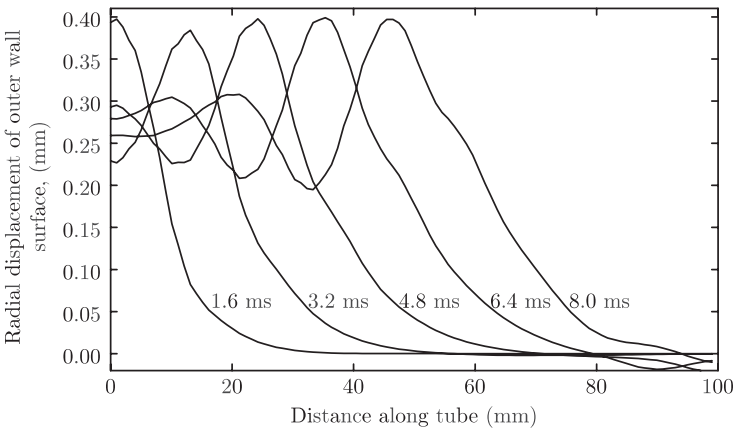

Figure 7. Radial displacement of outer wall surface at 1.6, 3.2, 4.8, 6.4 and 8.0 ms.

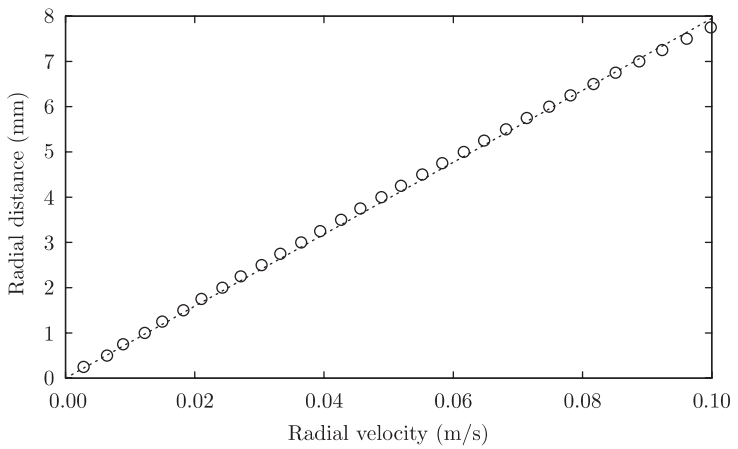

Figure 8. Radial velocity at $x = 50$ mm, $t = 6.4$ ms.

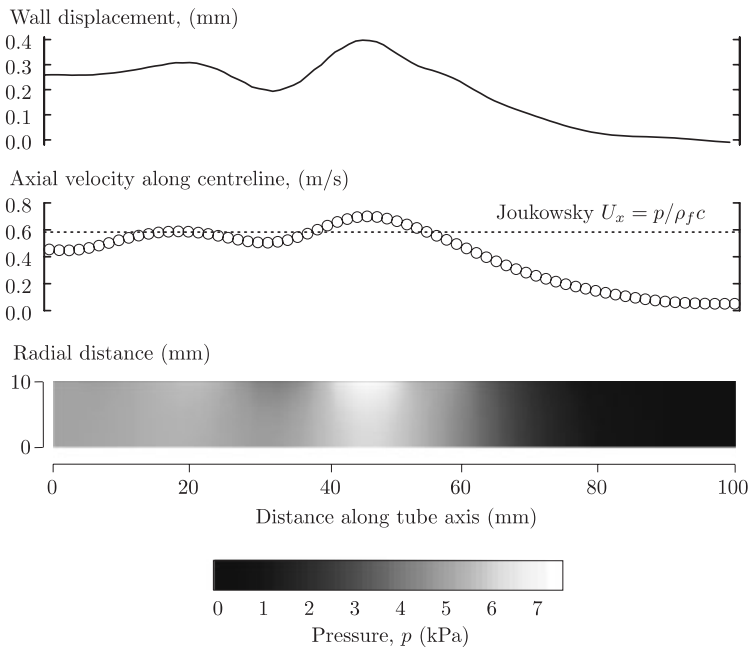

Figure 9. Comparison of wall displacement (top) and pressure distribution at 8.0 ms.

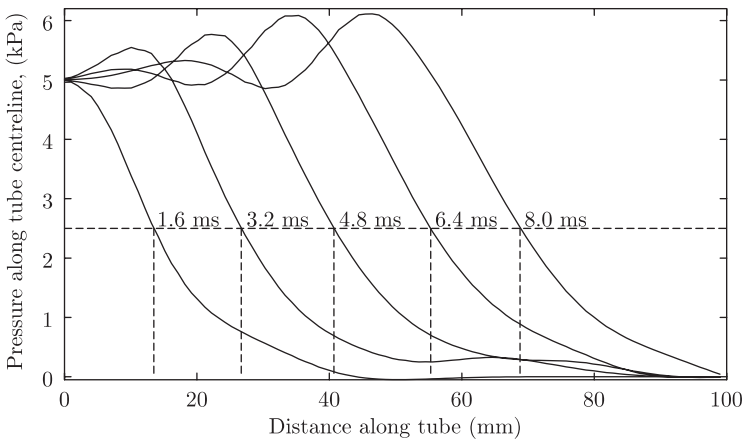

Figure 10. Pressure along the tube centerline.

fluid mass is

$$f = \frac{1}{2\pi}\sqrt{\frac{4E}{D^2\rho_s(1+M_{fs})}} \tag{29}$$

where different assumptions lead to a choice of expressions for the ratio of equivalent fluid mass to solid mass M_{fs}:

$$M_{\mathrm{fs}} = \begin{cases} \dfrac{D}{4t}\dfrac{\rho_{\mathrm{f}}}{\rho_{\mathrm{s}}}, & \text{for equivalent mass 'A' = total fluid mass [30]} \\ \dfrac{D}{6t}\dfrac{\rho_{\mathrm{f}}}{\rho_{\mathrm{s}}}, & \text{for equivalent mass 'B'<total fluid mass [31]} \\ \dfrac{D}{8t}\dfrac{\rho_{\mathrm{f}}}{\rho_{\mathrm{s}}}, & \text{for equivalent mass 'C'<total fluid mass [30]} \end{cases} \tag{30}$$

For our test case, Equation (29) gives: 269 Hz using equivalent mass A; 308 Hz using equivalent mass B; and, 336 Hz using equivalent mass C. These values are, respectively, 15% lower, 3% lower and 6% higher than the simulated frequency. The comparison immediately supports the view that only a fraction of the total mass of fluid contributes to radial motion. The alternative solutions for equivalent masses B and C assume a linear distribution of the radial fluid velocity. Figure 8 confirms the validity of this assumption since the radial velocity data follows closely the dotted line representing a linear distribution, in a region of radial expansion at a cross-section 50 mm along the tube axis at $t = 6.4$ ms.

Figure 9 shows the particle flow speed U_x along the tube centreline. Over the length of the tube, the flow speed compares reasonably well with Joukowsky's equation (4). It overshoots the Joukowsky flow speed in the region of largest radial displacement, most probably because of the fluid inertia. Figure 9 also shows the pressure distribution in the radial–axial plane at 8.0 ms, where a region of high pressure, shown as white on the grey-scale colourmap, occurs adjacent to the tube wall in the region of maximum wall deflection. The high-pressure region travels with the wave front at a level of ~ 7.6 kPa, 2.6 kPa above the excitation pressure of 5.0 kPa. It is most probably caused by compression generated in the fluid as it decelerates around the region of peak flow speed. The pressure monitored at the tube centreline provides the clearest image of wave propagation as shown in Figure 10. A mean propagation speed was estimated for the five meshes by a simple time of flight of the wave front defined as at the half-height of the pressure step, or 2.5 kPa. By plotting the mean wave speed versus number of cells in Figure 11, we conclude that the solution for the 70-40-7 mesh, 8.58 m/s, is within 0.25% of the solution extrapolated to infinity. The result is compared to a more precise analytical solution for wave speed than that given by Equation (3) in which the tube wall is not assumed to be 'thin' (e.g. Reference [32]) and a factor ϕ accounts for axial stress waves in the pipe wall, rather than assuming that the axial stress is fixed over the entire pipe [33]. The solution is

$$c = \phi\sqrt{\frac{K_{\mathrm{f}}}{\rho_{\mathrm{f}}}\left[1 + \left(\frac{(D+2t)^2}{t(D+t)} - 2(1-\nu)\right)\frac{K_{\mathrm{f}}}{E}\right]^{-1}} \tag{31}$$

where

$$\phi = \sqrt{1-\nu^2\left[1 + \frac{E}{K_{\mathrm{f}}}\frac{t}{D}\left(1 - \frac{K_{\mathrm{f}}}{E}\frac{\rho_{\mathrm{s}}}{\rho_{\mathrm{f}}}\right)\right]^{-1}} \tag{32}$$

For the test case $\phi = 0.95$, and the wave speed is $c = 8.77$ m/s. This analytical solution is approximately 2% higher than the wave speed predicted numerically.

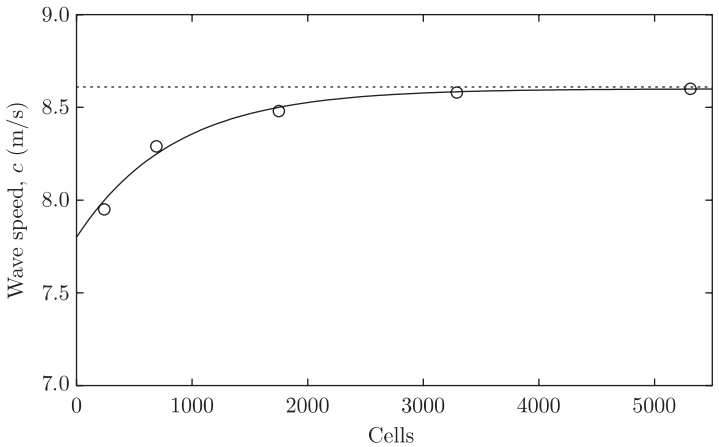

Figure 11. Predicted wave speed versus mesh size.

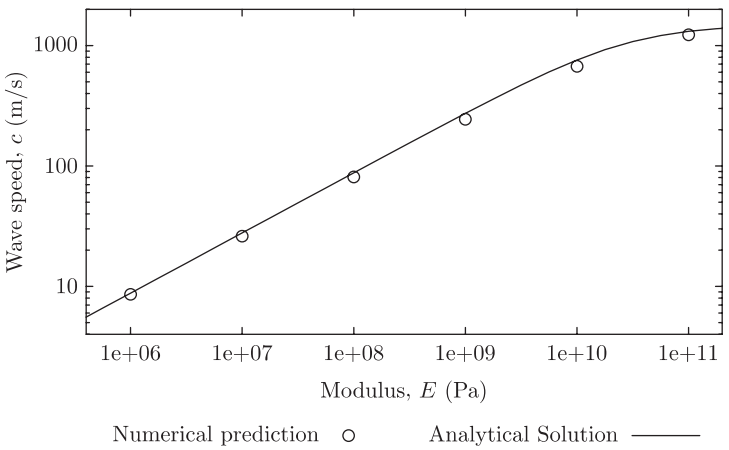

Figure 12. Predicted wave speed versus modulus.

The 70-40-7 mesh was then adopted to evaluate wave speed for subsequent cases in which E was increased successively by a factor of 10 over a range of tube wall modulus $10^6 \leqslant E \leqslant 10^{11}$ Pa. In each case, the mean propagation speed was extracted from the pressure data as described previously and the results are plotted in Figure 12 against the analytical solution given by Equations (31) and (32). The numerical solution is lower than the analytical solution by 2–10% over the range of E. This level of discrepancy seems reasonable given that the analytical method assumes a step profile in pipe wall displacement across the wave front which enables the tube to move radially at infinite speed, whereas momentum limits radial motion in the numerical approach, causing the wave speed to be lower.

6. DISCUSSION

This is the first stage of development of a new procedure for analysing FSI or general continuum systems. The main feature of the method is the derivation of a single set of equations for the continuum which are solved within a single discretized continuum domain, or mesh. The method has been shown to work on a purely structural case and has been used to predict wave propagation in flexible tubes. No additional approximations are made to the basic continuum model for Hookean solid and Newtonian fluid, and so it is possible to resolve detailed solutions for the test cases. This analysis of fluid transients in flexible tubes can be distinguished from most others in one respect: it *predicts* wave propagation from the pressure change at the inlet boundary, rather than *prescribing* wave-like behaviour by applying a time-varying velocity boundary condition, as in many studies in hemodynamics.

The method achieves its aim to overcome problems of instability associated with coupling by containing the interface within the solution domain. Figure 12 demonstrates the method to work effectively over the complete range of FSI regimes: from those dominated by fluid inertia in which $E \gg K$; through an intermediate regime in which $E \approx K$; and, to those dominated by the compliance of the tube wall in which $E \ll K$. The predictions for wave speed are highly credible and may actually provide useful estimates of the accuracy of analytical solutions.

There is great scope for further development of the method for more realistic modelling of hemodynamics and other applications. The model has many features which are well suited to complex material modelling:

- This formulation lends itself to modelling incompressible solids since the hydrostatic pressure has been separated from the stress tensor [34]. The implementation is somewhat straightforward since a constant density condition can be implemented within the continuity equation for the solid region as it is commonly done in fluid analyses. It uses implicit pressure-velocity coupling, without the need without the need for treating the solid as 'nearly' incompressible to prevent problems such as node locking [35].
- A large strain solid model can be implemented by moving the mesh with little cost to the computation. An Arbitrary Eulerian–Lagrangian approach would be most suitable in this case, in which the solid cells are moved with their current velocity, thereby reducing the convection to zero, and the fluid cells are deformed accordingly to maintain spatial continuity. OpenFOAM supports this approach.
- Complex constitutive models can arguably be implemented more easily using a velocity formulation than a displacement one. For example, simple damping can be introduced to a linear elastic solid through an increase in the coefficient μ_c which generates energy dissipation in the system and is a direct representation of a Kelvin–Voigt solid model.

REFERENCES

1. Korteweg DJ. Über die Fortplanzungsgeschwindigkeit des Schalles in elastischen Röhren. *Annalen der Physik und Chemie* 1878; **5**:525–542.
2. Streeter VL, Wylie EB. *Fluid Mechanics*. McGraw-Hill: New York, 1979.
3. Young T. Hydraulic investigations, subservient to an intended croonian lecture on the motion of blood. *Philosophical Transactions of the Royal Society of London* 1808; **98**:164–186.

4. Joukowsky N. Über den hydraulischen Stoss in Wasserleitungsröhren. *Mémoires de l'Académie Impériale des Sciences de St.-Pétersbourg*, *1900*, *Series 8* 1898; **9**(5).
5. Reuderink PJ, Hoogstraten HW, Sipkema P, Hillen B, Westerhof N. Linear and nonlinear one-dimensional models of pulse wave transmission at high Womersley numbers. *Journal of Biomechanics* 1989; **22**: 819–827.
6. Hilbert D. An efficient Navier–Stokes solver and its application to fluid flow in elastic tubes. *Colloquia Mathematica Societatis Janos Bolyai* 1986; **50**:439–447.
7. Steinman DA, Ethier CR. The effect of wall distensibility on flow in a two-dimensional end-to-side anastomosis. *Journal of Biomechanical Engineering—Transactions of the ASME* 1994; **116**:294–301.
8. Perktold K, Rappitsch G. Computer simulation of local blood flow and vessel mechanics in a compliant carotid artery bifurcation model. *Journal of Biomechanics* 1995; **28**:845–856.
9. Zhao SZ, Xu XY, Collins MW. The numerical analysis of fluid-solid interactions for blood flow in arterial structures. Part 2: development of coupled fluid-solid algorithms. *Proceedings of the Institution of Mechanical Engineers*, *Part H* 1998; **212**:241–252.
10. Tang D, Yang C, Ku DN. A 3-D thin-wall model with fluid–structure interactions for blood flow in carotid arteries with symmetric and asymmetric stenoses. *Computers and Structures* 1999; **72**:357–377.
11. Bathe M, Kamm RD. A fluid–structure interaction finite element analysis of pulsatile blood flow through a compliant stenotic artery. *Journal of Biomechanical Engineering—Transactions of the ASME* 1999; **121**: 361–369.
12. Henry FS, Collins MW. A novel predictive model with compliance for arterial flow. *Advances in Bioengineering—American Society of Mechanical Engineers* 1993; **BED26**:131–135.
13. Greenshields CJ, Weller HG, Ivanković A. The finite volume method for coupled fluid flow and stress analysis. *Computer Modeling and Simulation in Engineering* 1999; **4**:213–218.
14. Demirdzić I, Martinović D. Finite volume method for thermo-elastic-plastic stress analysis. *Computer Methods in Applied Mechanics and Engineering* 1993; **109**:331–349.
15. Demirdzić I, Muzaferija S. Finite volume method for stress analysis in complex domains. *International Journal for Numerical Methods in Engineering* 1994; **37**:3751–3766.
16. Jasak H, Weller HG. Application of the finite volume method and unstructured meshes to linear elasticity. *International Journal for Numerical Methods in Engineering* 2000; **48**(2):267–287.
17. Chow P, Cross M. An enthalpy control volume unstructured mesh (CV-UM) algorithm for solidification by conduction only. *International Journal for Numerical Methods in Engineering* 1992; **35**:1849–1870.
18. Demirdzić I, Muzaferija S. Numerical method for coupled fluid flow, heat transfer and stress analysis using unstructured moving meshes with cells of arbitrary topology. *Computer Methods in Applied Mechanics and Engineering* 1995; **125**:235–255.
19. Bailey C, Taylor GA, Cross M, Chow P. Discretization procedures for multi-physics phenomena. *Journal of Computational and Applied Mathematics* 1999; **103**:3–17.
20. Malvern LE. *Introduction to the Mechanics of a Continuous Medium*. Prentice-Hall: Englewood Cliffs, NJ, 1969.
21. Ferziger JH, Peric M. *Computational Methods for Fluid Dynamics*. Springer: Berlin, Germany, 1996.
22. Jasak H, Weller HG, Gosman D. High resolution NVD differencing scheme for arbitrarily unstructured meshes. *International Journal for Numerical Methods in Fluids* 1999; **31**:431–449.
23. Issa RI. Solution of the implicitly discretized fluid flow equations by operator-splitting. *Journal of Computational Physics* 1986; **62**:40–65.
24. Rhie CM, Chow WL. A numerical study of the turbulent flow past an isolated airfoil with trailing edge separation. *AIAA-82-0998*, *AIAA/ASME 3rd Joint Thermophysics*, *Fluids*, *Plasma and Heat Transfer Conference*, St. Louis, MO, 1982.
25. Hageman LA, Young DM. *Applied Iterative Methods*. Academic Press: New York, 1981.
26. Weller HG, Tabor G, Jasak H, Fureby C. A tensorial approach to continuum mechanics using object-oriented techniques. *Computers in Physics* 1998; **12**:620–631.
27. Ugural AC, Fenster SK. *Advanced Strength and Applied Elasticity*. Prentice-Hall: Englewood Cliffs, NJ, 1994.
28. Géradin M, Rixen D. *Mechanical Vibrations*. Wiley: Chichester, U.K., 1997.
29. Pedley TJ. *The Fluid Mechanics of Large Blood Vessels*. Cambridge University Press: Cambridge, U.K., 1980.
30. Barez F, Goldsmith W, Sackman JL. Longitudinal waves in liquid-filled tubes—ii. Experiments. *International Journal of Mechanical Sciences* 1979; **21**:223–236.

31. Kellner A, Schönfelder C. Die bedeutung der fluid/struktur-wechselwirkung für die druckstoßbelastung von rohrleitungen. *3R International* 1982; **21**:443–449.
32. Wylie EB, Streeter VL. *Fluid Transients in Systems*. Prentice-Hall: Englewood Cliffs, NJ, 1993.
33. Stuckenbruck S, Wiggert DC, Otwell RC. The influence of pipe motion on acoustic wave propagation. *Journal of Fluids Engineering—Transactions of the ASME* 1985; **107**:518–522.
34. Wheel MA. A mixed finite volume formulation for determining the small strain deformation of incompressible materials. *International Journal for Numerical Methods in Engineering* 1999; **44**:1843–1861.
35. Bathe K-J. *Finite Element Procedures*. Prentice-Hall: Englewood Cliffs, NJ 1997.

